Publ. Astron. Soc. Japan (2015) 67 (4), 59 (1–10)
doi: 10.1093/pasj/psu137
Advance Access Publication Date: 2015 February 28

Formation of young massive clusters from turbulent molecular clouds

Michiko S. Fujii[*,†]

Division of Theoretical Astronomy, National Astronomical Observatory of Japan, 2–21–1 Osawa, Mitaka-shi, Tokyo 181–8588, Japan

*E-mail: michiko.fujii@nao.ac.jp

[†]NAOJ Fellow

Received 2014 September 15; Accepted 2014 October 20

Abstract

Young massive clusters are as young as open clusters but more massive and compact compared with typical open clusters. The formation process of young massive clusters is still unclear, and it is an open question whether the formation process is the same for typical open clusters or not. We perform a series of *N*-body simulations starting from initial conditions constructed from the results of hydrodynamical simulations of turbulent molecular clouds. In our simulations, both open clusters and young massive clusters form when we assume a density-dependent star-formation efficiency. We find that a local star-formation efficiency higher than 50% is necessary for the formation of young massive clusters, but open clusters form from less dense regions with a local star formation efficiency of $< 50\%$. We confirm that the young massive clusters formed in our simulations have mass, size, and density profile similar to those of observed young massive clusters such as NGC 3603 and Trumpler 14. We also find that these simulated clusters evolve via hierarchical mergers of sub-clusters within a few mega years, as is suggested by recent simulations and observations. Although we do not assume initial mass segregation, we observe that the simulated massive clusters show a shallower slope of the mass function ($\Gamma \sim -1$) in the cluster center compared to that of the entire cluster ($\Gamma \sim -1.3$). These values are consistent with those of some young massive clusters in the Milky Way such as Westerlund 1 and Arches.

Key words: galaxies: star clusters: general — methods: numerical — open clusters and associations: general — open clusters and associations: individual (Arches, NGC 3603, Trumpler 14, Westerlund 1, Westerlund 2)

1 Introduction

Young massive clusters (YMCs) such as NGC 3603, Westerlund 1 and 2 in the Milky Way (MW) and R 136 in the Large Magellanic Cloud have been found, and their detailed structures have been studied over the past 10 years. YMCs are as young as open clusters ($\lesssim 20$ Myr) but as dense as globular clusters ($\sim 10^4\,M_\odot\,\mathrm{pc}^{-3}$). The typical mass of YMCs in the MW is $\sim 10^4\,M_\odot$, which is slightly less massive than typical globular clusters (Portegies Zwart et al. 2010). They populate mainly in the galactic disk, and some of them (e.g., Arches and Quintuplet) are located close to the galactic center. Thus, YMCs seem to be a population different from typical open clusters, but it is still unclear whether their formation process is the same as that of open clusters or not.

In our previous papers, we performed a series of N-body simulations and found that a formation scenario via hierarchical mergers of sub-clusters is preferable for YMCs in order to explain their dynamically mature characteristics (core collapse, mass segregation, and runaway stars) (Fujii et al. 2012; Fujii & Portegies Zwart 2013). In these studies, however, we adopted the simple but artificial initial conditions of merging sub-clusters with a mass of $\sim 5000\,M_\odot$. In contrast to such a simple model of N-body simulations, observed star-forming regions always show more complicated clumpy and filamentary structures (Gutermuth et al. 2009; Schneider et al. 2012; Kainulainen et al. 2014).

In order to model more realistic initial conditions for N-body simulations, several methods have been attempted. Hydrodynamical simulations of collapsing molecular clouds including star formation and stellar feedback (e.g., Bonnell et al. 2003, 2008; Bate 2012; Federrath & Klessen 2012; Federrath et al. 2014; Dale et al. 2014) are the most straightforward approach. Such simulations, however, involve huge simulation costs to resolve individual star formation. Therefore, no simulation large enough for the formation of massive clusters with mass of $\sim 10^4\,M_\odot$ has been performed yet. Compared with such hydrodynamical simulations, performing pure N-body simulations is numerically much cheaper, and therefore it enables us to treat a large number of stars. However, the initial distribution of stars we should adopt is unclear. Allison et al. (2009, 2010) adopted fractal initial conditions, which naturally form clumpy structures similar to observed star-forming regions. For the velocity structure of the obtained system, they therefore gave a random velocity distribution locally following a Gaussian.

An intermediate approach was attempted by Moeckel and Bate (2010). They first performed a hydrodynamical simulation of a turbulent molecular cloud which includes star formation using sink particles. After about one free-fall time of the initial gas cloud, they stopped the hydrodynamical simulations, removed all residual gas assuming instantaneous gas expulsion, and continued pure N-body simulations using a direct N-body code. This kind of approach seems to work successfully. In Fujii and Portegies Zwart (2015) we adopted a similar method. We also performed a hydrodynamical simulation using a smoothed-particle hydrodynamics (SPH) method but with a lower resolution in order to avoid using sink particles. After about one free-fall time, we stopped the hydrodynamical simulation and replaced gas particles with stellar particles, assuming a star-formation efficiency depending on the local gas density. Then, we removed all residual gas particles and continued a pure N-body simulation using a direct N-body code. With this method, we can construct initial conditions for N-body simulations based on turbulent molecular clouds, which are also more massive than previous works.

In Fujii and Portegies Zwart (2015), we demonstrated that an ensemble of star clusters obtained from our simulations successfully reproduce observed ones in the Carina region and nearby (< 1 kpc from the Sun). The most massive clusters formed in the simulations had a mass of $\sim 10^4\,M_\odot$, which is as massive as YMCs in the MW. In this paper, we investigate the detailed formation and evolution of YMCs in our simulations and compare the structures to those of observed YMCs and open clusters in the MW.

2 Simulations

Our simulations consist of following three steps: (1) hydrodynamical simulations of turbulent molecular clouds, (2) star formation following the gas density obtained from the hydrodynamical simulations, and (3) pure N-body simulations of stars based on the structure of the molecular clouds.

We perform hydrodynamical simulations using an SPH code, `Fi` (Hernquist & Katz 1989; Gerritsen & Icke 1997; Pelupessy et al. 2004; Pelupessy 2005), with the Astronomical Multipurpose Software Environment (AMUSE: Portegies Zwart et al. 2013; Pelupessy et al. 2013). For initial conditions of molecular clouds, we follow those in Bonnell, Bate, and Vine (2003) and adopt an isothermal homogeneous gas sphere with a divergence-free random Gaussian velocity field δv with a power spectrum $|\delta v|^2 \propto k^{-4}$ (Ostriker et al. 2001). The spectral index of -4 appears in the case of compressive turbulence (Burgers turbulence), and recent observations of molecular clouds (Heyer & Brunt 2004) and numerical simulations (Federrath et al. 2010; Roman-Duval et al. 2011; Federrath 2013a) also suggested values similar to -4. We adopt the total gas mass and size of $4.1 \times 10^5\,M_\odot$ and 10 pc, respectively, which give the mean density of $\sim 1700\,\mathrm{cm}^{-3}$ ($\sim 100\,M_\odot\,\mathrm{pc}^{-3}$) assuming that the mean weight per particle is $2.33\,m_\mathrm{H}$. As a consequence, the free-fall time (t_ff) of the gas cloud is 0.83 Myr. We set the gas temperature at 30 K and assume zero total energy (potential plus kinetic energy is zero). We adopt the mass of SPH particles of $1\,M_\odot$, which is equal to the mean stellar mass of the following N-body simulations. The gravitational softening length is 0.1 pc. We set the number of particles within a smoothing length as 64. With these settings, the smallest length scale we can resolve is ~ 0.6 pc, which is smaller than the typical size of embedded clusters (1 pc) (Lada & Lada 2003) but slightly larger than the observed typical width of gas filaments (~ 0.1 pc) (Arzoumanian et al. 2011). In this simulation, we cannot resolve individual star formation, we can

Table 1. Initial conditions. $M_{\rm gas}$, $r_{\rm gas}$, $\rho_{\rm gas}$ are the mass, radius, and density of the molecular cloud, respectively.*

Model	$M_{\rm gas}$ ($M_\odot$)	$r_{\rm gas}$ (pc)	$\rho_{\rm gas}$ ($M_\odot\,{\rm pc}^{-3}$)	SFE	$\rho_{\rm c}$ ($M_\odot\,{\rm pc}^{-3}$)	$M_{\rm star}$ ($M_\odot$)	$N_{\rm star}$	ϵ	$\epsilon_{\rm d}$	Q
A1	4.1×10^5	10	100	eq. (1)	–	3.2×10^4	31895	0.078	0.22	2.6
A2	4.1×10^5	10	100	eq. (1)	–	4.3×10^4	42596	0.096	0.25	0.85
A3	4.1×10^5	10	100	eq. (1)	–	2.3×10^4	23273	0.057	0.16	8.4
B1	4.1×10^5	10	100	0.8	5×10^3	3.4×10^4	33974	0.083	0.30	1.6
B2	4.1×10^5	10	100	0.8	5×10^3	4.3×10^4	42710	0.10	0.30	0.84
C1	4.1×10^5	10	100	0.3	10^3	3.4×10^4	34086	0.084	0.30	4.2
C2	4.1×10^5	10	100	0.3	10^3	4.4×10^4	43500	0.11	0.30	2.9
A-1M	1.0×10^6	13.4	100	eq. (1)	–	1.1×10^5	109080	0.11	0.27	1.8

*SFE and $\rho_{\rm c}$ indicate the SFE and the critical density for the constant SFE. $M_{\rm star}$ and $N_{\rm star}$ are the total mass and number of stars for N-body simulations. ϵ and $\epsilon_{\rm d}$ are the SFE for the entire system and the region with a local density of $>1000\,M_\odot\,{\rm pc}^{-3}$, respectively. Q is the virial ratio of stellar particles at the beginning of N-body simulations. If $Q=1.0$, the system is in virial equilibrium

treat dense gas clumps in which star formation is expected to occur.

After $0.9t_{\rm ff}$, we stop the hydrodynamical simulations and analyze the density distribution of the collapsed molecular cloud. We replace the densest SPH particles with stellar particles by adopting the local star-formation efficiency (SFE), $\epsilon_{\rm loc}$, which depends on the local gas density ρ given by

$$\epsilon_{\rm loc}=\alpha_{\rm sfe}\sqrt{\frac{\rho}{100\,(M_\odot\,{\rm pc}^{-3})}}, \quad (1)$$

where $\alpha_{\rm sfe}$ is a coefficient which controls the SFE and is a free parameter in our simulations. This choice of SFE is motivated by the recent result that the star formation rate scales with free-fall time (Krumholz et al. 2012; Federrath 2013b). We adopt $\alpha_{\rm sfe}=0.02$ in order to reproduce observed SFEs. In Krumholz, Dekel, and McKee (2012), an SFE per $t_{\rm ff}$ of 0.015 is obtained. With these settings, we obtain a global SFE for the entire regions of several per cent and an SFE of dense regions ($>1000\,M_\odot\,{\rm cm}^{-3}$) of 20%–30%, which is consistent with observations (Lada & Lada 2003) and also simulations of molecular clouds with star formation (Federrath & Klessen 2013). The global SFE (ϵ) and the SFE of the dense region ($\epsilon_{\rm d}$) for the individual models are summarized in table 1 as model A. We perform three runs with different random seeds for the turbulence for model A, and they are named A1, A2, and A3. After replacing gas particles with stellar particles, we randomly assign stellar masses following the Salpeter mass function (Salpeter 1955) with a lower and upper cut-off mass of 0.3 and 100 $M_\odot$. The mass does not conserve locally, but conserves globally. The positions and velocities of the stellar particles are identical to those of the SPH particles.

We also adopt two models with a constant SFE only for dense regions for a comparison. One is a constant SFE of 0.8 for the regions with $\rho>5000\,M_\odot\,{\rm pc}^{-3}$ (model B), and the other is a a constant SFE of 0.3 for the regions with $\rho>1000\,M_\odot\,{\rm pc}^{-3}$ (model C). While model C follows an assumption that the SFE cannot exceed 50%, model B is motivated by recent numerical study that in a sub-cluster on a length-scale of 0.1–0.2 pc the fraction of gas is less than 10% (Kruijssen et al. 2012; Moeckel et al. 2012). For both models, the values of the total stellar mass, ϵ, and $\epsilon_{\rm d}$ are very similar to those of model A. These models are also summarized in table 1. We perform two runs with different random seeds for the turbulence for model B (B1 and B2) and C (C1 and C2). A1, B1, and C1, and A2, B2, and C2 have the same random seed, respectively. In addition, we adopt a model that is the same as model A but with a total gas mass of $10^6\,M_\odot$. We call this model as A-1M.

After replacing gas particles with stellar particles, we remove all residual gas particles, assuming an instantaneous gas expulsion, and perform pure N-body simulations with only stars up to 10 Myr (but 4 Myr for model A-1M because of the calculation cost). For N-body simulations we adopt a sixth-order Hermite scheme (Nitadori & Makino 2008) without any gravitational softening. We include stellar collisions with a sticky sphere approximation with stellar radius of zero-age main-sequence following the description of Hurley, Pols, and Tout (2000). We also include stellar mass-loss at the end of the main-sequence lifetime following Hurley, Pols, and Tout (2000) (see Fujii et al. 2009 and Fujii & Portegies Zwart 2015 for the details). We use a time-step criterion of Nitadori and Makino (2008) with an accuracy parameter of $\eta=0.1$–0.25. The energy error was $\lesssim10^{-3}$ for all simulations over the entire duration of the simulations.

3 Formation and evolution of star clusters

In figure 1 we present the snapshots at $t=0$, 2, 4, and 10 Myr for models A1, B1, and C1. Hereafter, we set the beginning of N-body simulations as $t=0$. Since these

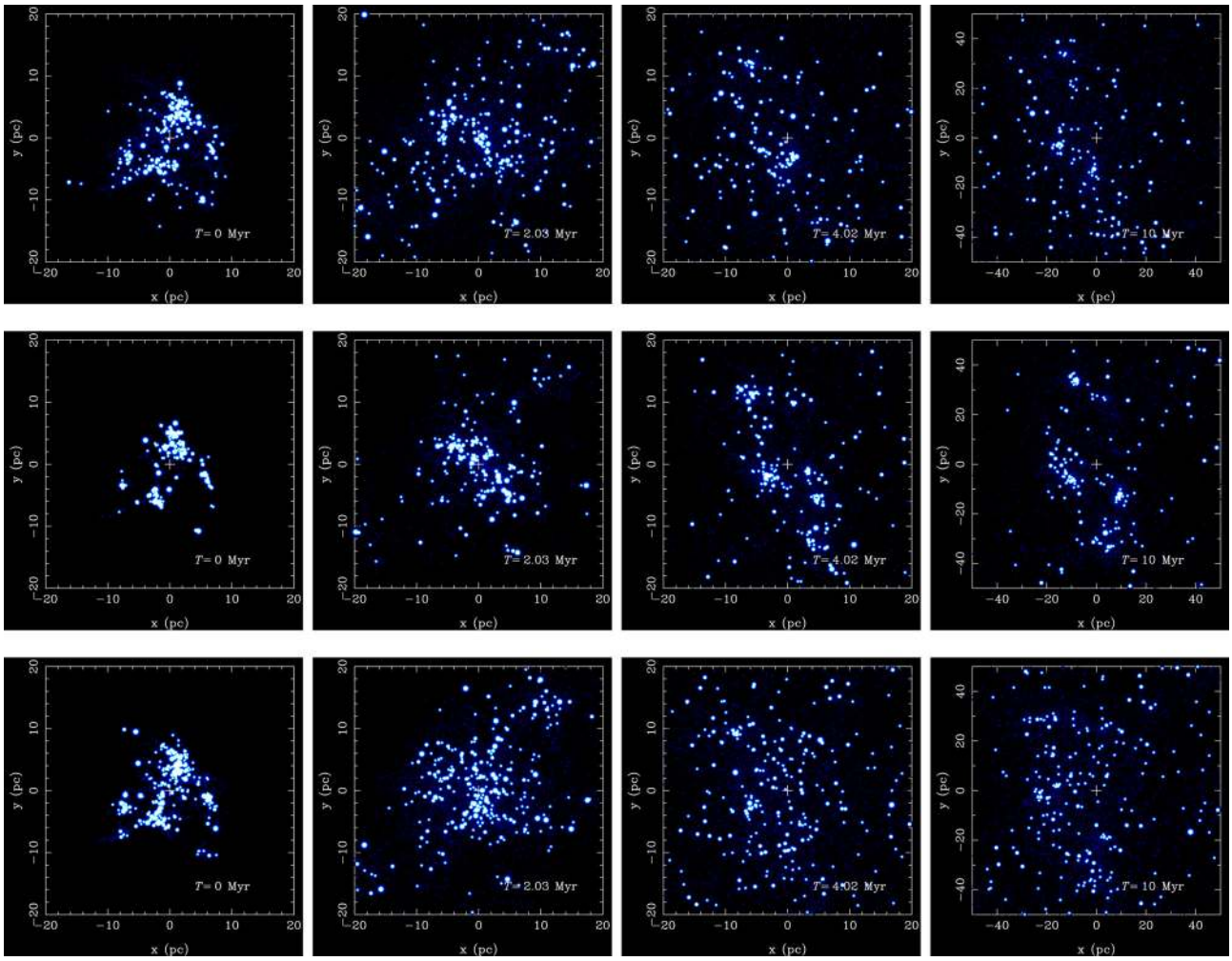

Fig. 1. Snapshots at $t = 0$, 2, 4, and 10 Myr for models A1, B1, and C1 from top to bottom. (Color online)

models have the same random seed for the turbulence, the initial distributions of stars are very similar. At $t = 2$ Myr, some massive star clusters form especially in models A1 and B1. In model C1, the final distribution of stars is more elongated and the formed clusters are smaller than those in models A1 and B1. In this section, we detect the clusters formed in our simulation and investigate their time evolution.

3.1 Mass–radius diagram of star clusters

At $t = 0.5$, 2, 4, and 10 Myr, we interrupt the simulations and detect star clusters using a clump finding method, HOP (Eisenstein & Hut 1998), in the AMUSE framework. We adopt the following parameters: the outer cut-off density of $\rho_{\rm out} = 4.5 M_{\rm s}/(4\pi r_{\rm h}^3)$ (three times the half-mass density of the entire system, $\rho_{\rm h}$), the saddle density threshold of $8\rho_{\rm out}$, the peak density threshold of $10\rho_{\rm out}$, the number of particles for neighbor search of $N_{\rm dense} = 64$, the number of particles to calculate the local density of $N_{\rm hop} = 64$, and the number of neighbor particles in order to determine for two groups to merge of $N_{\rm merge} = 4$. With this set-up, the detection limit of the clump mass is $\sim 100\,M_\odot$. Since HOP sometimes detected multiple clumps as one clump, we apply the HOP method again for the detected clumps if the half-mass density of the clump ($\rho_{\rm h,c}$) is less than $100\rho_{\rm h}$, adopting $\rho_{\rm out} = \rho_{\rm h,c}$. If $\rho_{\rm h,c} > 100\rho_{\rm h}$, such a clump is compact and therefore does not seem to contain multiple clumps. We confirmed that no detected clumps contain multiple clumps.

In figure 2 we present the mass–radius diagram of the detected clusters at each time. We also plot observed young star clusters in the MW. Most of the simulated clusters are located in the bottom left-hand region in this diagram. Clusters in this region are observationally categorized as open or embedded clusters. Embedded clusters are very young and, therefore, they are still covered by surrounding molecular clouds. Typical mass and size is $100\,M_\odot$ and ~ 1 pc, respectively (Lada & Lada 2003). The distribution of open and embedded clusters shifts to the upper region in the

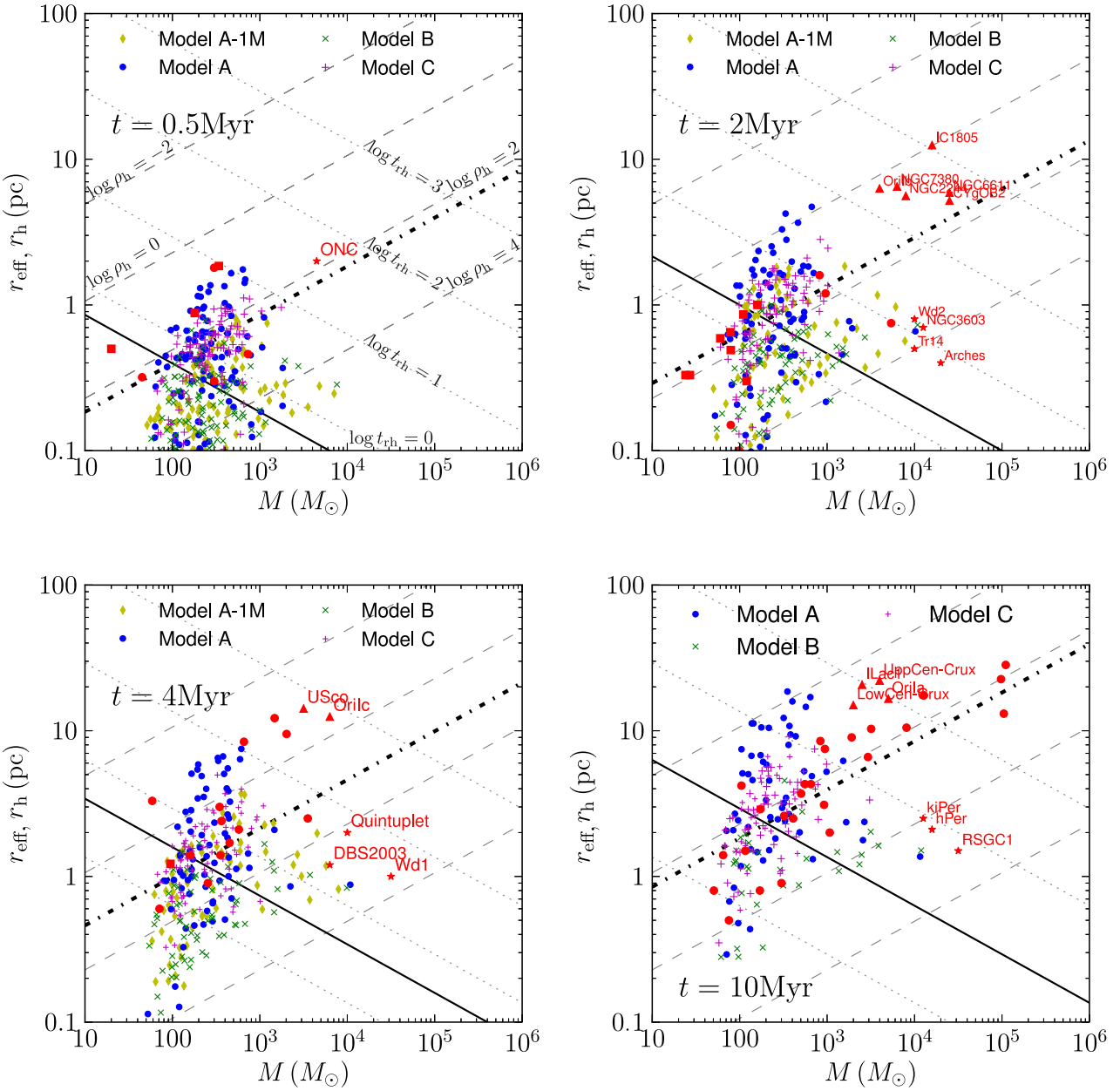

Fig. 2. Mass–radius diagram of clusters obtained from the simulations at 0.5, 2, 4, and 10 Myr. Same models with different random seeds are plotted with the same symbols. Red points indicate observed MW clusters with ages of ≤1 Myr, 1–3 Myr, 3–6 Myr, and 6–15 Myr. Squares, circles, stars, and triangles are for embedded, open, young massive (Portegies Zwart et al. 2010) and leaky clusters, respectively. The data is obtained from the followings: Lada and Lada (2003); Piskunov et al. (2008); Pfalzner (2009); Portegies Zwart, McMillan, and Gieles (2010); Winston et al. (2009); Luhman et al. (2003); Andersen et al. (2006); Fang et al. (2009); Levine et al. (2006); Flaherty and Muzerolle (2008); Bonatto and Bica (2011); Horner, Lada, and Lada (1997); Drew et al. (1997); Hodapp and Rayner (1991). We assumed that the age of embedded clusters given in Lada and Lada (2003) is 1 Myr. The observed clusters and associations with the names are given in Portegies Zwart, McMillan, and Gieles (2010). Black thick solid and dash–dotted lines indicate the line at which the relaxation time and the dynamical time are equal to the age. (Color online)

diagram with time. This is due to the dynamical evolution of star clusters. Gieles, Heggie, and Zhao (2011) modeled the dynamical evolution of star clusters based on Hénon's model (Hénon 1961, 1965). After the first mass segregation (or core collapse) phase, star clusters expand due to the energy generation in the core. In this expansion phase, the half-mass relaxation time ($t_{\rm rh}$) increases with the cluster age ($t_{\rm age}$), and $t_{\rm rh} \sim t_{\rm age}$. In the figure, we indicate the half-mass relaxation time for a given mass and half-mass radius with gray dotted lines. We adopt

$$t_{\rm rh} \sim 2 \times 10^8 \left(\frac{M}{10^6\ M_\odot}\right)^{1/2} \left(\frac{r_{\rm h}}{1\ {\rm pc}}\right)^{3/2} {\rm yr} \qquad (2)$$

assuming $r_{\rm vir} \sim r_{\rm h}$ and $\langle m \rangle = 1\,M_\odot$ (Portegies Zwart et al. 2010). The black thick lines in figure 2 indicate the line at which $t_{\rm rh} = t_{\rm age}$. Open and embedded clusters are mainly located around this line and evolve with it. Such dynamical evolution of open clusters is also seen in simulations performed by Moeckel et al. (2012). Since the initial relaxation time of the open and embedded clusters are around 1 Myr, they dynamically evolve immediately and shift to the expansion phase. From the evolution in this diagram, embedded clusters seem to be ancestors of typical open clusters.

YMCs distribute an area clearly different from that of open and embedded clusters. They are located at the middle right of the mass–radius diagram ($\sim 10^4\,M_\odot\,{\rm pc}^{-3}$ and ~ 1 pc) at $t = 2$, 4, and 10 Myr. In our simulations, we also find a branch of cluster distribution similar to YMCs, although the number of such dense massive clusters is much smaller compared to the main distribution of clusters similar to open clusters. We treat these massive ($\sim 10^4\,M_\odot$) clusters as YMCs and compare them to observed YMCs in section 4.

The third population of clusters distribute at the top right-hand region in the mass–radius diagram. They are "leaky" clusters (Pfalzner 2009) but can also be categorized as "association" because they seem to be unbound systems (Portegies Zwart et al. 2010). They are as massive as YMCs but much less dense. In this diagram, especially at $t = 10$ Myr, the leaky clusters seem to populate at the high-mass end of open and embedded clusters.

Portegies Zwart, McMillan, and Gieles (2010) proposed to use the ratio of the age and dynamical time ($t_{\rm dyn}$) of clusters as an indicator of bound systems. The dynamical time is given as

$$t_{\rm dyn} \sim 2 \times 10^4 \left(\frac{M}{10^6\ M_\odot}\right)^{-1/2} \left(\frac{r_{\rm h}}{1\ {\rm pc}}\right)^{3/2} {\rm yr} \qquad (3)$$

(Portegies Zwart et al. 2010), assuming $r_{\rm vir} \sim r_{\rm h}$. If $t_{\rm dyn}$ is much shorter than the cluster age ($t_{\rm age}$), the cluster seems to be bound. If $t_{\rm dyn}$ is comparable to $t_{\rm age}$ or is even longer, the cluster seems to be unbound. Portegies Zwart, McMillan, and Gieles (2010) suggested that if $t_{\rm age}/t_{\rm dyn} < 3$, the system is unbound. With this criterion, they categorized the leaky clusters as associations (unbound systems). The black dash–dotted lines in figure 2 indicate the density with which the dynamical time of the cluster is equal to the age. Most of the MW open clusters are located near the boundary, and therefore they seem to be loosely bound (or some of them may not be bound). While most open clusters and embedded clusters distribute around the line with $t_{\rm age} = t_{\rm rh}$, leaky clusters and some massive open clusters (they might be a population that is the same as the leaky clusters) distribute far away from this line. This means that the leaky and typical open clusters are dynamically in different evolutionary phases.

In our simulation, no cluster similar to the leaky clusters forms. Is it possible to form leaky clusters (or associations) in the same process we adopted? The maximum mass of star clusters formed in a turbulent molecular cloud is expected to increase with the mass of the molecular cloud (Fujii & Portegies Zwart 2015). If we increase the initial gas mass, the distribution of open clusters might elongate toward the leaky clusters. In model A-1M, which has $10^6\,M_\odot$ of the initial gas mass, we found a larger number of YMCs compared with model A, but the mass of open clusters was not much different from those of model A. Another possibility is that we fail to detect leaky clusters because of our clump finding method. Maíz-Apellániz (2001) categorized young massive stellar systems (< 20 Myr and $> 3 \times 10^4\,M_\odot$) in local galaxies, evaluating their morphology using one-quarter, one-half, and three-quarters light-radii. Some clusters in their sample were categorized as "scaled OB associations," which do not have clear centers but show asymmetric, elongated, and clumpy structures. The typical size of the scaled OB associations is a few tens of parsecs, which is comparable to those of the leaky clusters. Some leaky clusters are also known as sub-clustered systems (Wright et al. 2014). Using our clump finding method, such clumpy clusters could be detected as some smaller clumps instead of a large clumpy system.

3.2 Formation of young massive clusters via hierarchical mergers

As we see in the previous subsection, the majority of clusters evolve upward in the mass–radius diagram due to the relaxation. Some clusters, however, especially massive clusters, increase their mass and move from left to right in the diagram. We find that these massive clusters experienced hierarchical mergers. In figure 3, we present the merger history of the most massive cluster in model A. The cluster finally evolved to a cluster which has a radius and mass similar to those of a YMC (~ 1 pc and $\sim 10^4\,M_\odot$). During 10 Myr, this cluster accumulated 17 smaller clusters, but most of the mergers occurred before 4 Myr.

Such a formation scenario via hierarchical mergers is preferable for YMCs. Observed YMCs show dynamically mature features such as mass segregation and the existence of runaway stars, which occur on the relaxation time scale. The relaxation time obtained from their current mass and size, however, implies that they are too young to show such dynamically mature features. Merger scenarios can overcome this discrepancy. Since smaller clusters in general have a shorter relaxation time, they can dynamically evolve within a few Myr. If such smaller sub-clusters assemble in

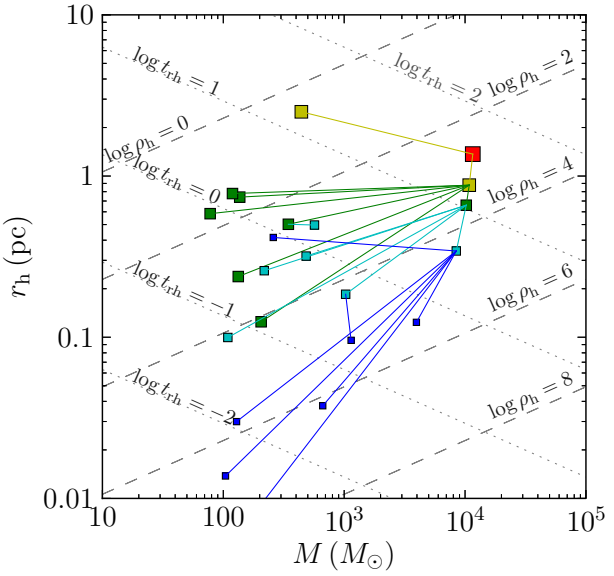

Fig. 3. Merger history for in mass–radius diagram for the most massive cluster in model A. Blue, cyan, green, yellow, and red squares indicate clusters at 0.25, 0.5, 2, 4, and 10 Myr, respectively. The lines indicate the assembling and the evolution of the clusters. (Color online)

a few Myr and form a massive cluster, the merged cluster shows dynamically evolved features which are taken over from the sub-clusters. In Fujii et al. (2012) we demonstrated that the degree of mass segregation, the distribution of massive stars, and the formation of runaway stars in observed YMCs are successfully explained by the assembling of sub-clusters. Observationally, a remnant of sub-clusters was found in the vicinity of R 136 (Sabbi et al. 2012).

In figure 3 the first cluster is very dense but has a short relaxation time, less than 1 Myr. If the cluster failed to experience a merger with other dense sub-clusters, it would evolve to a less dense cluster on its relaxation timescale. If, however, the cluster merged with other dense sub-clusters before it becomes less dense, the cluster can evolve into a more massive cluster, maintaining its high density. After repeated mergers, the relaxation time exceeds 10 Myr at $t = 2$ Myr, and therefore the dynamical evolution slows down. In section 4, we discuss the detailed structure of this massive cluster and compare it with observed YMCs.

3.3 The effect of the star-formation efficiency

In figure 2 we see that the distribution of detected clusters in our simulation depends on the model for the SFE; only open clusters form in model C, while YMCs form in model B. In model A (density-dependent SFE), both populations form at the same time. In the middle and bottom panels in figure 1, we present the snapshots of models B and C. While massive clusters are seen in models A and B, model C shows a less clumpy structure. We perform clump findings at each time and the mass and size of the obtained clusters are plotted in figure 2. As seen in figure 1, model C does not form any YMC-type clusters, but in model B the formed clusters mainly distribute the YMC brunch.

These differences of cluster formation modes are caused by the local SFE we assumed. In model C, all clusters are dominated by gas when they form because we adopt a constant SFE of 30%. These clusters always become less dense after gas expulsion. In models A or B, however, the densest regions are allowed to be dominated by stars, and as a consequence, dense clumps can maintain their high density over gas expulsion. The dense clumps can merge with each other before they evolve to less dense clusters due to the two-body relaxation, and can finally grow up to become dense massive clusters. With a density-dependent SFE such as we assumed, the local SFE exceeds 50% when $\rho > 6.3 \times 10^4\,M_\odot\,{\rm pc}^{-3}$. This value is roughly consistent with the density of observed YMCs ($\rho \sim \times 10^4\,M_\odot\,{\rm pc}^{-3}$, see figure 2). Thus, we conclude that a local SFE higher than 50% is necessary for the formation of YMCs and that a density-dependent SFE (i.e., a constant SFE per free-fall time) is preferable to explain the formation of both open clusters and YMCs in the same mechanism.

4 Properties of YMCs in simulations

In the previous section, we showed that YMC-like clusters form in our simulations. Are they really comparable to YMCs in the MW? In figure 4 we present the surface density profiles of the largest cluster in model A at 2 and 4 Myr. The total mass and the half-mass radius are $1.1 \times 10^4\,M_\odot$ and 0.88 pc at 2 Myr, respectively, which are very similar to those of NGC 3603 ($1.3 \times 10^4\,M_\odot$ and 0.70 pc) (Portegies Zwart et al. 2010). The spikes at around 1 pc at 2 Myr are sub-clumps merging to the main cluster, and they disappear at 4 Myr. We measure the core radius and density using a local density method of Casertano and Hut (1985). The original method is applied for volume densities, but we here apply it for surface densities.

Using this method, we obtained the core radius of 0.21 pc for all stars. We also measured the core radius only for stars with $m > 1\,M_\odot$, because less massive stars are not detected in observations, and obtained a core radius of 0.19 pc. These values are comparable to that of NGC 3603: 0.45 pc in Eisenhauer et al. (1998) and 0.15 pc in Portegies Zwart, McMillan, and Gieles (2010). The core densities of the simulated clusters are 1.9×10^4 and 4.5×10^3 star pc^{-2} for all stars and for $> 1\,M_\odot$ stars, respectively. The core density for stars with $> 1\,M_\odot$ is also comparable to the observed one (see figure 8 in Eisenhauer et al. 1998). Trumpler 14 is also a young massive cluster

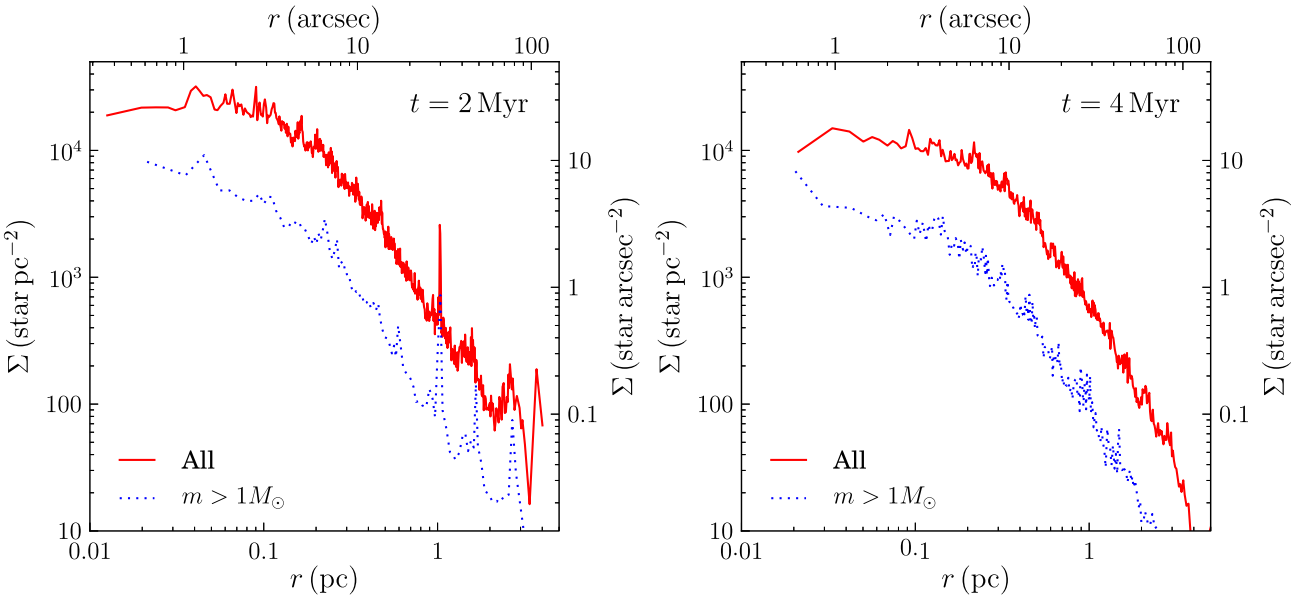

Fig. 4. Projected stellar density of the most massive cluster in model A at 2 (left) and 4 (right) Myr. Right and top axes are in arcsec and star arcsec^{-2} assuming that the cluster exists at the distance of NGC 3603. We assume that $1'' = 0.035$ pc (Eisenhauer et al. 1998). Red full and blue dashed curves indicate the projected density profile for all stars and stars with $> 1\,M_\odot$, respectively. The core radii are 0.21 and 0.19 pc for all and $> 1\,M_\odot$ stars, respectively. (Color online)

which has a mass, size, and age similar to NGC 3603 (see top-right panel of figure 2). The surface density profile is observationally obtained, and the radius and surface density of the core are estimated to be 0.11–0.22 pc and 4×10^3–1.1×10^4 star pc^{-2}, respectively (Sana et al. 2010). These values are also consistent with those obtained from our simulations. At $t = 4$ Myr, the core becomes larger and the density decreases. The core density and radius are 9.3×10^3 star pc^{-2} and 0.31 pc for all stars and 2.6×10^3 star pc^{-2} and 0.25 pc for stars with $m > 1\,M_\odot$.

Although we did not take into account any initial mass segregation, the formed clusters are mass-segregated, as are YMCs. In figure 5 we present the mass function of the massive cluster shown in figure 4 in a sequence of increasing annuli at 2 and 4 Myr. We obtain the slope of the mass function (Γ) using a least-squares fit. For the fitting, we include only the data points with $\log_{10} m > 0.5$, where m is the stellar mass, because most of the observational data are complete down to a few solar masses (Pang et al. 2013). We find that the slope of the mass function tends to be steeper as the annuli are increasing. (Note that the power-law slope at $1 < r < 2$ pc at 2 Myr is also shallow, but this is caused by a sub-cluster in this annulus.) This trend is clear especially in the inner most annulus ($r < 0.25$ pc), and the slope is $\Gamma \sim -1$ ($\Gamma = -1.35$ for Salpeter mass function, which is the initial mass function we assume). Such shallower mass functions in inner annuli are commonly observed in YMCs in the MW such as NGC 3603 (Pang et al. 2013), Westerlund 1 (Lim et al. 2013), and Arches (Habibi et al. 2013). The values of slopes are different in each YMC; $\Gamma = -0.88$ for total and $\Gamma = -0.26$ for $r \lesssim 0.2$ pc for NGC 3603 (Pang et al. 2013), $\Gamma = -1.4$ (Gennaro et al. 2011) or $\Gamma = -0.8$ in total and $\Gamma = -1.1$ for $r \lesssim 0.3$ pc for Westerlund 1 (Lim et al. 2013), and $\Gamma = -1.53$ for total and $\Gamma = -0.5$ for $r < 0.2$ pc for Arches (Habibi et al. 2013), respectively.

The mass segregation proceeds in a relaxation time. The relaxation time obtained from the current masses and sizes of YMCs in the MW is ~ 10 Myr (see figure 2), which is longer than their age. If these YMCs formed via mergers as is seen in our simulations, their ancestor sub-clusters would have had a much shorter relaxation time of less than 1 Myr (see figure 3). Since the dynamically mature features remain after mergers (Fujii et al. 2012; Fujii & Portegies Zwart 2013), the mass segregation in the YMCs seems to be a natural consequence of the dynamical evolution via mergers.

5 Summary

We performed a series of direct N-body simulations of young star clusters starting from initial conditions constructed from hydrodynamical simulations of turbulent molecular clouds. In our simulations, we obtained an ensembles of young star clusters. Most of them had a mass and size similar to those of typical open clusters in the MW. In the mass–radius diagram, most of the simulated clusters and observed open and embedded clusters distribute around a point at which the relaxation time and the dynamical time

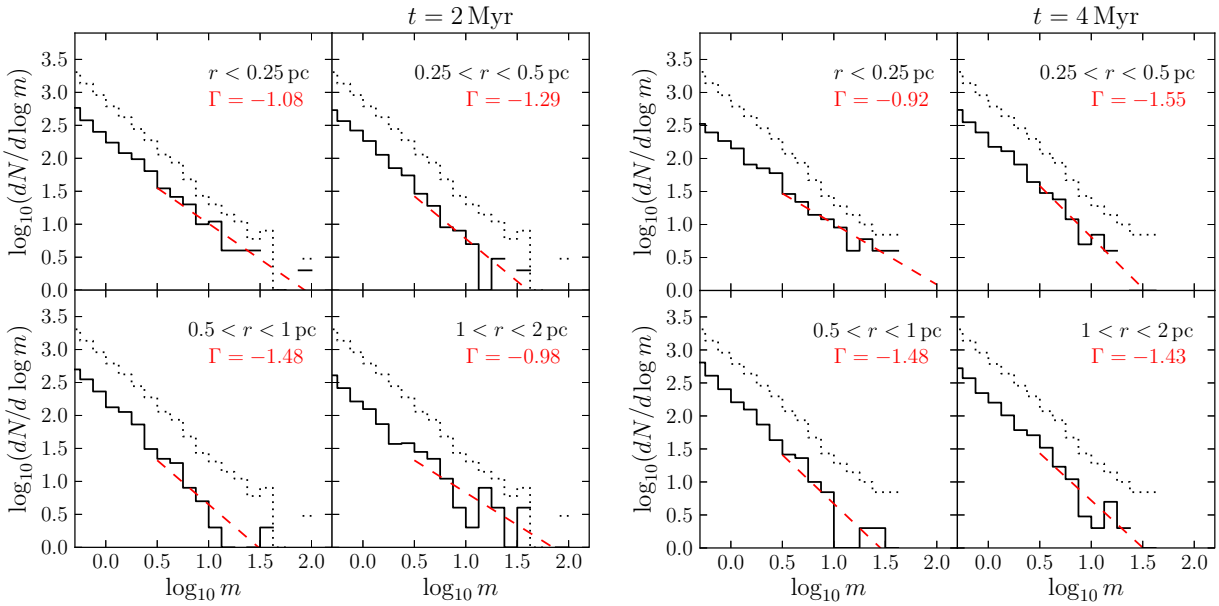

Fig. 5. Mass function of the most massive cluster in model A in a sequence of increasing annuli at 2 (left) and 4 Myr (right). The dotted histogram is the total mass function within 2 pc. Red dashed line indicates the result of a least-square fit for the data points with $\log_{10} m > 0.5$. The slope of the mass function is indicated as Γ. The slope of the total mass function obtained from the fitting is $\Gamma = -1.34$ and -1.31 for 2 and 4 Myr, respectively. (Color online)

are similar to the cluster age. This suggests that embedded and open clusters are the same population (i.e., embedded clusters are the ancestors of open clusters) and that they are in the expansion phase after mass segregation. Observed leaky clusters and some open clusters are located near or slightly above the line on which the dynamical time is equal to the age, but far away from the line on which the relaxation time is equal to the age. They therefore seems to be in an evolution phase dynamically different from typical open and embedded clusters.

Most of the clusters formed in our simulations evolve to clusters similar to open clusters. Some clusters, however, experience hierarchical mergers and evolve to dense massive clusters which have characteristics similar to those of YMCs in the MW. We find that a local star-formation efficiency of more than $\sim 50\%$ is necessary for the formation of YMCs. This result is consistent with that of Pfalzner and Kaczmarek (2013), in which YMCs are suggested to form with an SFE of 60%–70%. If the local SFE is always less than 50%, only open clusters form instead. This result suggests that the center of dense star-forming clumps which evolves to form YMCs is almost gas-free as is also suggested by recent simulations (Kruijssen et al. 2012; Moeckel et al. 2012). A local SFE that is dependent on the local density (i.e., free-fall time) (Krumholz et al. 2012; Federrath 2013b) is preferable for the formation of both open and young massive clusters in the same process.

Massive dense clusters formed in our simulation evolved via hierarchical mergers within a first few mega years. Since smaller clumps have a shorter relaxation time, the merger remnant of smaller clumps shows dynamically mature features such as mass segregation, even if we initially assign the stellar mass irrespective of their positions. We confirmed that the surface density profile of our simulated cluster is actually consistent with that of observed YMCs such as NGC 3603 and Trumpler 14. We also find that the slope of the stellar mass function is shallower in the cluster center due to the mass segregation. This feature is also observed in YMCs in the MW (Pang et al. 2013; Lim et al. 2013; Habibi et al. 2013).

Acknowledgments

The author thanks Tsuyoshi Inoue and the anonymous referee for useful comments on the manuscript. This work was supported by JSPS KAKENHI Grant Number 26800108 and NAOJ Fellowship. Numerical computations were partially carried out on Cray XC30 at the Center for Computational Astrophysics (CfCA) of the National Astronomical Observatory of Japan and Little Green Machine at Leiden Observatory.

References

Allison, R. J., Goodwin, S. P., Parker, R. J., de Grijs, R., Portegies Zwart, S. F., & Kouwenhoven, M. B. N. 2009, ApJ, 700, L99

Allison, R. J., Goodwin, S. P., Parker, R. J., Portegies Zwart, S. F., & de Grijs, R. 2010, MNRAS, 407, 1098

Andersen, M., Meyer, M. R., Oppenheimer, B., Dougados, C., & Carpenter, J. 2006, AJ, 132, 2296

Arzoumanian, D., et al. 2011, A&A, 529, L6
Bate, M. R. 2012, MNRAS, 419, 3115
Bonatto, C., & Bica, E. 2011, MNRAS, 414, 3769
Bonnell, I. A., Bate, M. R., & Vine, S. G. 2003, MNRAS, 343, 413
Bonnell, I. A., Clark, P., & Bate, M. R. 2008, MNRAS, 389, 1556
Casertano, S., & Hut, P. 1985, ApJ, 298, 80
Dale, J. E., Ngoumou, J., Ercolano, B., & Bonnell, I. A. 2014, MNRAS, 442, 694
Drew, J. E., Busfield, G., Hoare, M. G., Murdoch, K. A., Nixon, C. A., & Oudmaijer, R. D. 1997, MNRAS, 286, 538
Eisenhauer, F., Quirrenbach, A., Zinnecker, H., & Genzel, R. 1998, ApJ, 498, 278
Eisenstein, D. J., & Hut, P. 1998, ApJ, 498, 137
Fang, M., van Boekel, R., Wang, W., Carmona, A., Sicilia-Aguilar, A., & Henning, T. 2009, A&A, 504, 461
Federrath, C. 2013a, MNRAS, 436, 1245
Federrath, C. 2013b, MNRAS, 436, 3167
Federrath, C., & Klessen, R. S. 2012, ApJ, 761, 156
Federrath, C., & Klessen, R. S. 2013, ApJ, 763, 51
Federrath, C., Roman-Duval, J., Klessen, R. S., Schmidt, W., & Mac Low, M.-M. 2010, A&A, 512, A81
Federrath, C., Schrön, M., Banerjee, R., & Klessen, R. S. 2014, ApJ, 790, 128
Flaherty, K. M., & Muzerolle, J. 2008, AJ, 135, 966
Fujii, M., Iwasawa, M., Funato, Y., & Makino, J. 2009, ApJ, 695, 1421
Fujii, M. S., & Portegies Zwart, S. 2013, MNRAS, 430, 1018
Fujii, M. S., & Portegies Zwart, S. 2015, MNRAS, 449, 726
Fujii, M. S., Saitoh, T. R., & Portegies Zwart, S. F. 2012, ApJ, 753, 85
Gennaro, M., Brandner, W., Stolte, A., & Henning, T. 2011, MNRAS, 412, 2469
Gerritsen, J. P. E., & Icke, V. 1997, A&A, 325, 972
Gieles, M., Heggie, D. C., & Zhao, H. 2011, MNRAS, 413, 2509
Gutermuth, R. A., Megeath, S. T., Myers, P. C., Allen, L. E., Pipher, J. L., & Fazio, G. G., 2009, ApJS, 184, 18
Habibi, M., Stolte, A., Brandner, W., Hußmann, B., & Motohara, K. 2013, A&A, 556, A26
Hénon, M. 1961, Ann. Astrophys., 24, 369
Hénon, M. 1965, Ann. Astrophys., 28, 62
Hernquist, L., & Katz, N. 1989, ApJS, 70, 419
Heyer, M. H., & Brunt, C. M. 2004, ApJ, 615, L45
Hodapp, K.-W., & Rayner, J. 1991, AJ, 102, 1108
Horner, D. J., Lada, E. A., & Lada, C. J. 1997, AJ, 113, 1788
Hurley, J. R., Pols, O. R., & Tout, C. A. 2000, MNRAS, 315, 543
Kainulainen, J., Federrath, C., & Henning, T. 2014, Science, 344, 183
Kruijssen, J. M. D., Maschberger, T., Moeckel, N., Clarke, C. J., Bastian, N., & Bonnell, I. A. 2012, MNRAS, 419, 841
Krumholz, M. R., Dekel, A., & McKee, C. F. 2012, ApJ, 745, 69
Lada, C. J., & Lada, E. A. 2003, ARA&A, 41, 57
Levine, J. L., Steinhauer, A., Elston, R. J., & Lada, E. A. 2006, ApJ, 646, 1215
Lim, B., Chun, M.-Y., Sung, H., Park, B.-G., Lee, J.-J., Sohn, S. T., Hur, H., & Bessell, M. S. 2013, AJ, 145, 46
Luhman, K. L., Stauffer, J. R., Muench, A. A., Rieke, G. H., Lada, E. A., Bouvier, J., & Lada, C. J. 2003, ApJ, 593, 1093
Maíz-Apellániz, J. 2001, ApJ, 563, 151
Moeckel, N., & Bate, M. R. 2010, MNRAS, 404, 721
Moeckel, N., Holland, C., Clarke, C. J., & Bonnell, I. A. 2012, MNRAS, 425, 450
Nitadori, K., & Makino, J. 2008, New Astron., 13, 498
Ostriker, E. C., Stone, J. M., & Gammie, C. F. 2001, ApJ, 546, 980
Pang, X., Grebel, E. K., Allison, R. J., Goodwin, S. P., Altmann, M., Harbeck, D., Moffat, A. F. J., & Drissen, L. 2013, ApJ, 764, 73
Pelupessy, F. I. 2005, PhD thesis, Leiden University
Pelupessy, F. I., van der Werf, P. P., & Icke, V. 2004, A&A, 422, 55
Pelupessy, F. I., van Elteren, A., de Vries, N., McMillan, S. L. W., Drost, N., & Portegies Zwart, S. F. 2013, A&A, 557, A84
Pfalzner, S. 2009, A&A, 498, L37
Pfalzner, S., & Kaczmarek, T. 2013, A&A, 559, A38
Piskunov, A. E., Kharchenko, N. V., Schilbach, E., Röser, S., Scholz, R.-D., & Zinnecker, H. 2008, A&A, 487, 557
Portegies Zwart, S. F., McMillan, S. L. W., & Gieles, M. 2010, ARA&A, 48, 431
Portegies Zwart, S., McMillan, S. L. W., van Elteren, E., Pelupessy, I., & de Vries, N. 2013, Comput. Phys. Commun., 183, 456
Roman-Duval, J., Federrath, C., Brunt, C., Heyer, M., Jackson, J., & Klessen, R. S. 2011, ApJ, 740, 120
Sabbi, E., et al. 2012, ApJ, 754, L37
Salpeter, E. E. 1955, ApJ, 121, 161
Sana, H., Momany, Y., Gieles, M., Carraro, G., Beletsky, Y., Ivanov, V. D., de Silva, G., & James, G. 2010, A&A, 515, A26
Schneider, N., et al. 2012, A&A, 540, L11
Winston, E., et al. 2009, AJ, 137, 4777
Wright, N. J., Parker, R. J., Goodwin, S. P., & Drake, J. J. 2014, MNRAS, 438, 639